Carbohydrate Polymers 190 (2018) 121–128

Contents lists available at ScienceDirect

Carbohydrate Polymers

journal homepage: www.elsevier.com/locate/carbpol

Insights into gelation kinetics and gel front migration in cation-induced polysaccharide hydrogels by viscoelastic and turbidity measurements: Effect of the nature of divalent cations

Uyen T.D. Huynh[a,b], Odile Chambin[a,c], Aline Maire du Poset[a], Ali Assifaoui[a,c,*]

[a] Univ. Bourgogne Franche-Comté, AgroSup Dijon, PAM UMR A 02.102, F-21000 Dijon, France
[b] University of Technology and Education, University of Danang, 48 Cao Thang, Da Nang, Viet Nam
[c] Department of Pharmaceutical Technology, School of Pharmacy, Univ. Bourgogne Franche-Comté, 7 Bd. Jeanne d'Arc, 21079 Dijon, France

ARTICLE INFO

Keywords:
Hydrogel
Calcium
Zinc
Magnesium
Barium
Polygalacturonic acid
Diffusion coefficient
Gelation mechanism
Turbiscan

ABSTRACT

Polysaccharide-based hydrogels were prepared by the diffusion of various divalent cations (X^{2+}) into the polygalacturonate (polyGal) solution through a dialysis membrane. The diffusion of various divalent cations (Mg^{2+}, Ca^{2+}, Zn^{2+} and Ba^{2+}) was investigated. The polyGal gel growth was studied as a function of the initial cation concentration by both viscoelastic and turbidity measurements. We have demonstrated for the first time that the determination of the spatiotemporal variation of turbidity during the gelation process allowed to study the gel front migration. For Ca-polyGal, Zn-polyGal and Ba-polyGal, the gel front migration was characterized by the presence of a peak at the sol/gel interface. This peak was not observed in the case of Mg-polyGal where the gel was not formed. The apparent diffusion coefficient of the gel front (D_{app}) which was calculated from the evolution of this peak increased when the initial cation concentration was increased. Moreover, we have suggested a gelation mechanism based on the presence of a threshold molar ratio R* (= $[X^{2+}]$/[Galacturonic unit]) in which some point-like crosslinks are precursors of the formation of dimers and multimers inducing the contraction of the gel and thus the formation of the gel front.

1. Introduction

Polymer hydrogels have received considerable attention in the biomaterials science because of their applications in drug delivery, tissue engineering, and biosensor fields (Li & Mooney, 2016). Hydrogels are three-dimensional cross-linked polymeric networks which have the ability to imbibe large amounts of water and to swell without dissolving (Vashist, Vashist, Gupta, & Ahmad, 2014). Among numerous polymers, anionic polysaccharides such as pectin and alginate remain attractive polymers due to their low toxicity, biocompatibility and availability. The most useful property of these charged polysaccharides is their ability to form gels in the presence of divalent cations such as Ca^{2+}. Pectin is an anionic polysaccharide that has linear regions formed by D-galacturonic acid (GalA) monomers, linked by α-(1,4) glycosidic bonds, and branched regions formed with a various type of neutral monosaccharides linked together (Thibault & Rinaudo, 1985). The GalA units have carboxyl groups, which may be present as free carboxyl groups or methyl-esterified groups depending on the origin, isolation, and processing of pectin.

Calcium-induced polysaccharide gel can be prepared in two different ways: internal and external gelation processes. The internal gelation consists of the diffusion of Ca^{2+} inside the polysaccharide solution by using an inactivated form of calcium such as Ca-EDTA and $CaCO_3$ (Stokke et al., 2000). The release of calcium ions is then triggered by the decrease of the pH by using hydrolyzing molecules (e.g. δ-gluconolactone). This gelation mode induces the formation of isotropic gels. The external gelation occurs by the diffusion of divalent cations, through a dialysis membrane, from a large outer reservoir into the polysaccharide solution. In this case, the gel exhibits an inhomogeneous polymers distribution (Maire du Poset, Lerbret, Zitolo, Cousin, & Assifaoui, 2018; Skjåk-Bræk, Grasdalen, & Smidsrød, 1989; Ström et al., 2007). Indeed, a gradual decrease of the polymer concentration is observed from the nearest to the farthest parts from the dialysis membrane (Mørch, Donati, & Strand, 2006; Skjåk-Bræk et al., 1989). Moreover, these gels exhibit anisotropic structure with a birefringence due to the molecular orientation as observed by several authors (Maki et al., 2014; Wu et al., 2011).

The gel formation between such polysaccharides and calcium ions exhibits a gelation front that subsequently progresses across the liquid polymer to leave gelled calcium-polysaccharide behind (Hills et al.,

* Corresponding author at: Univ. Bourgogne Franche-Comté, AgroSup Dijon, PAM UMR A 02.102, F-21000 Dijon, France.
E-mail address: ali.assifaoui@u-bourgogne.fr (A. Assifaoui).

https://doi.org/10.1016/j.carbpol.2018.02.046
Received 27 October 2017; Received in revised form 12 February 2018; Accepted 16 February 2018
Available online 21 February 2018
0144-8617/

2000). In this process, the diffusion and reaction compete and lead to the formation of a physical gel with controlled structure. Many authors have demonstrated that the diffusion of calcium ions through the gel network is dependent on the initial concentration of calcium ions, the ionic strength of the alginate solution and the size of pores formed in the gel (Caccavo, Ström, Larsson, & Lamberti, 2016; Hills et al., 2000; Kim, 1990; Potter, Balcom, Carpenter, & Hall, 1994; Skjåk-Bræk et al., 1989; Wu et al., 2014). The diffusion coefficient increased when the Ca^{2+} concentration increased. The increase in polymer concentration decreased the diffusion coefficient of Ca^{2+} due to the consumption of more cations for complexation and the gel matrix hinders the diffusion of free cations (Braschler et al., 2011; Thu et al., 2000). The localization and the characterization of the gel front migration during the gelation process was studied by using many techniques such as polarizing optical microscopy (Maki et al., 2014; Maki et al., 2011; Wu et al., 2014), magnetic resonance imaging (Hills et al., 2000; Skjåk-Bræk et al., 1989; Thu et al., 2000), fluorescence microscopy (Bjørnøy et al., 2016; Braschler et al., 2011; Mørch et al., 2006). The structure of such gel was studied by small angle x-ray and light scattering (SAXS), small angle neutron scattering (SANS) which gave information on the final organization of polymer chains and the size of the gel network in relation to its mechanical properties (Agulhon, Robitzer, Habas, & Quignard, 2014; Maki, Furusawa, Dobashi, Sugimoto, & Wakabayashi, 2017; Ventura, Jammal, & Bianco-Peled, 2013; Wu et al., 2011).

In this paper, we have developed a new method to study the gel front migration during the gelation of an anionic polysaccharide (sodium polygalacturonate noted polyGal). This method is based on the determination of the spatiotemporal variation of the turbidity in the polyGal sample during the gelation process by using a commercial instrument (Turbiscan®). The gelation process which occurred inside the Turbiscan® apparatus is due to the diffusion of the divalent cations (X^{2+}) through a dialysis membrane into the polyGal solution. PolyGal, which is the skeleton of the pectin, is an anionic linear homopolymer that can form a gel, in specific conditions, only via the formation of Gal-divalent cation-Gal bridges. We have studied the spatiotemporal variation of the turbidity for four divalent cations (Mg^{2+}, Zn^{2+}, Ca^{2+} and Ba^{2+}). It must be noted that the ionic radius of these cations increases in the following order: $Mg^{2+} \sim Zn^{2+} < Ca^{2+} < Ba^{2+}$. Mg^{2+} is a 'negative' reference since it is well known that this cation does not form gels in presence of pectin (Donati, Asaro, & Paoletti, 2009). We have chosen to study Zn^{2+}, because it has been used to design pectin drug delivery systems with specific properties (Assifaoui, Chambin, & Cayot, 2011; Assifaoui et al., 2015). We have established a state diagram in which the initial cation concentrations and the gelation time were varied from 10 to 750 mM and from 10 to 1440 min, respectively. The viscoelastic properties (G' and G") of the obtained hydrogels were then investigated by rheological measurements.

2. Materials and methods

2.1. Materials

Polygalacturonic acid (95% of purity, Mw ~ 50 kDa), calcium chloride dihydrate, and barium chloride were purchased from Sigma (St Louis, MO). Sodium chloride, zinc chloride, and magnesium chloride anhydrous were purchased from VWR, BDH Prolabo. All reagents were analytical grade.

2.2. Preparation of PolyGal gels

Polygalacturonic acid solution (10 gL^{-1} which corresponds to 55 mM of Gal unit) was prepared by dissolving the polygalacturonic acid powder in a solution of NaCl (10 mM). The concentration of the polysaccharide is close to the overlap concentration ($c^* = 12 \pm 2\ gL^{-1}$) as determined by viscosity measurements (Maire du Poset et al., 2018). The pH was adjusted to 5.5 with sodium hydroxide in order to have a fully negatively charged polysaccharide (polygalacturonate (polyGal)). Then, 10 mL of the viscous polyGal solutions were placed in a plastic box with an inner diameter of 3.8 cm and covered by a hydrated dialysis membrane (SnakeSkin®, with a cut-off of 10 kDa). This box was then immersed in a cross-linking solution containing divalent cations ($CaCl_2$, $ZnCl_2$, $BaCl_2$ and $MgCl_2$) at various concentrations (10, 50, 100, 250, 500 and 750 mM). All experiments were done at room temperature and in triplicate. For low divalent cation concentrations and short gelation time, gels were not formed for Zn^{2+}, Ca^{2+} and Ba^{2+}. For Mg^{2+}, polyGal did not form a consistent gel whatever the initial concentration of Mg^{2+} tested (< 750 mM) and the gelation time (24 h). For the obtained gels, the amount of dry matter ($m_{dried\ gel}$) was determined by drying the gel at 105 °C for 40 h. Taking into account the thickness of the gel (d) and the radius of the cylindrical gel which was constant (r = 1.9 cm), the gel density (ρ_{gel}) was determined according to the following equation (Eq. (1)).

$$\rho_{gel} = \frac{m_{dried\ gel}}{\pi \times r^2 \times d} \quad (1)$$

2.3. Rheological measurements

For each gel, the viscoelastic properties were recorded using a stress-controlled dynamic rheometer (MCR 302 from Anton Paar) equipped with parallel plates geometry with a diameter of 25 mm at controlled temperature (T = 25 °C). In order to maintain a good contact between the plate and the gel and to reduce potential adverse effects due to slipping, the normal force was adjusted to 0.5 N. The application of a larger normal force (1.5 N) induced a syneresis phenomenon. The elastic modulus (G') and the viscous modulus (G") were recorded for polyGal gels for each gelation time and as a function of the concentration of divalent cations. We firstly performed frequency sweep experiments from 0.5 to 100 rad s^{-1} at a fixed shear stress (τ = 50 Pa). Then, shear stress sweep experiments from 10 to 100 Pa at a fixed angular frequency (ω = 10 rad s^{-1}) were performed. These experiments allowed us to define the linear viscoelastic region (LVR), where the viscoelastic properties are independent of the angular frequency and the shear stress. Each experiment was triplicated in order to check the reproducibility and the coherence of registered data.

2.4. The gel front migration determination

During the gel formation, divalent cations (X^{2+}) diffused through the dialysis membrane and bound the polyGal chains. This binding induces changes in the turbidity of the polyGal solution. By using a Turbiscan® apparatus (Formulaction, France) with an adapted experimental lab-made set-up (Fig. 1), we were able to follow the evolution of the turbidity as a function of both the gelation time and the height of the gel. The Turbiscan device works with a pulsed near-infrared light source (λ = 880 nm) and two synchronous detectors for transmittance (at 180°) and backscattering (at 45°), which move up and down along a cylindrical glass tube containing the sample, with data collection every 40 μm (Bru et al., 2004). The experimental lab-made set-up is composed of two tubes with different diameters in order to put one tube inside the other (Fig. 1). The large tube was the standard Turbiscan tube; where 15 mL of polyGal solution (10 g L^{-1}) was introduced. The second tube contained the divalent cations solution with various concentrations. The two tubes were separated by a dialysis membrane (SnakeSkin®, with a cut-off of 10 kDa). In this case, the diffusion of the divalent cation occurred from the top to the bottom. The temperature inside the two tubes was around of 25 ± 2 °C. The light transmittance was recorded from the bottom to the top of the Turbiscan tube for various gelation time (0–24 h).

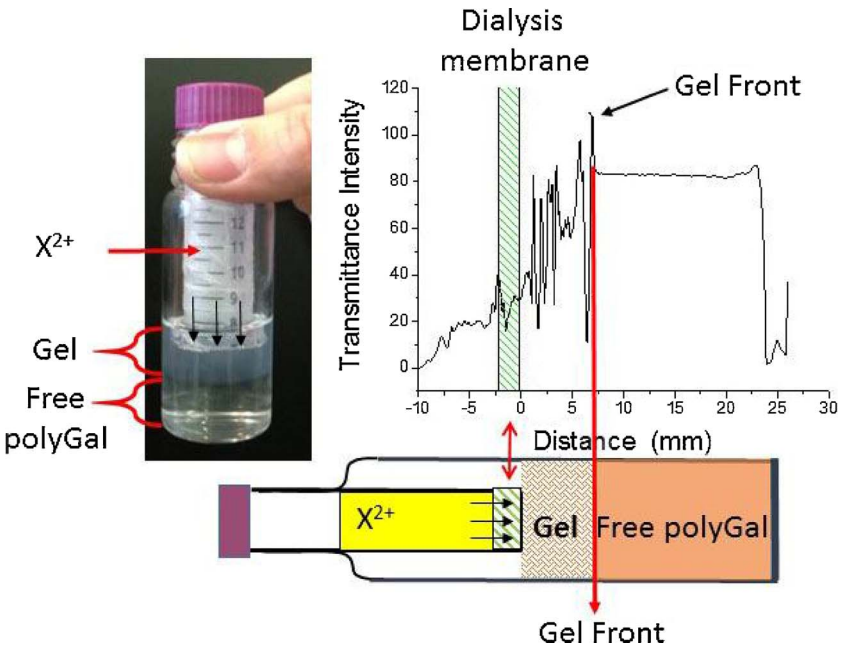

Fig. 1. Photo and schema representing the experimental lab-made set-up for measuring the gel front migration. The diffusion of the divalent cation (X^{2+}) occurred from the top to the bottom. The transmittance intensities were collected by the Turbiscan® device as a function of the gelation time (0–24 h) and at different heights of the tube. In the present figure, the transmittance intensity is recorded for a given gelation time.

3. Results and discussion

3.1. Phase diagram

For each divalent cation (Zn^{2+}, Ca^{2+}, Ba^{2+}), the formation of the polyGal gel depends on the gelation time and on the initial concentration of the divalent cation (Fig. 2a and Fig. S1 in Supplementary information). For Zn-polyGal, Ca-polyGal and Ba-polyGal gels, we have observed the presence of three regions (Fig. 2a and Fig. S1.1). In the region 1 (low gelation time and low cation concentration), the gel was brittle and its thickness was too thin to be measured correctly. In the region 2, whatever the nature of the divalent cation, the gel thickness was both time and cation concentration dependent (the gelation process was not fully finished). When the gelation was achieved (region 3), we have observed that the thickness of Ca-polyGal gels and Ba-polyGal gels were slightly higher than Zn-polyGal gels (Fig. S1.2). For the shorter gelation time ($t < 120$ min), whatever the calcium ions concentration, a linear relationship was observed between the square of the gel thickness (d^2) and the gelation time (t) (insert in Fig. 2b) according to the following equation of $d^2 = 2D_{app}t$ (Sherwood & Pigford, 1952; Skjåk-Bræk et al., 1989). The apparent diffusion coefficient (D_{app}) of the gel front can be determined by the slope of d^2/t. Thus, D_{app} values were equal to $15 \times 10^{-6}\,cm^2\,s^{-1}$, $21 \times 10^{-6}\,cm^2\,s^{-1}$ and $28 \times 10^{-6}\,cm^2\,s^{-1}$ for 250 mM, 500 mM and 750 mM, respectively. The increase of this coefficient with calcium concentration was previously observed by several authors (Bjørnøy et al., 2016; Braschler et al., 2011; Skjåk-Bræk et al., 1989; Wu et al., 2014). This linear relationship was also observed in the case of Ba-polyGal and Zn-polyGal and was observed only for short gelation times (< 120 min) (Fig. S1.2)

3.2. Characterization of the hydrogel: rheological properties

For each divalent cation (Zn^{2+}, Ca^{2+}, Ba^{2+}), the linear viscoelastic region (LVR) was determined for two types of hydrogels: the thinnest (100 mM/gelation time of 2.5 h) and the thickest (750 mM/gelation time of 17 h) (data are not shown). For all samples, the following conditions ($\omega = 10\,rad\,s^{-1}$ and $\tau = 50$ Pa which corresponds to 0.1 % of deformation) allowed us to compare the viscoelastic properties within the LVR region. The evolution of G' and G" for Ba-polyGal and Zn-polyGal are presented in Fig. S2 in SI. For the three polyGal gels, no crossover point between G' and G" was detected throughout the frequency range studied; whatever the divalent concentration and the gelation time (data not shown). The evolution of G' and G" as a function of gelation time was presented for two initial cation concentrations 250 and 750 mM (Fig. 3 and Fig. S2). It can be noted that the elastic contribution was predominant (G' > G"), whatever the calcium concentration and the gelation time. Moreover, the loss tangent (tan (δ) = G"/G') corresponding to the ratio of the viscous portion to elastic one, remained low (~0.2) and constant as the gelation time increased. As the gelation time was increased, elastic modulus increased progressively until reached a plateau at 60 kPa and 80 kPa for 250 mM and 750 mM of calcium cations, respectively (Fig. 3). The time at which this plateau appeared (t_p) was shorter for high cation concentration whatever the nature of the cation (~70 min for 750 mM and ~150 min for 250 mM). For Ba-polyGal, the G' and G" did not change significantly with the gelation time (Fig. S2). For high initial cation concentration (750 mM), the elastic modulus at the plateau of Ca-polyGal (G'_p ~ 80 kPa) was higher than those obtained with Zn-polyGal and Ba-polyGal (G'_p ~ 40 kPa) (Fig. S2b). The increase of calcium concentration induced an increase of the gel migration (Bjørnøy et al., 2016; Wu et al., 2014). The elastic modulus values obtained for the three polyGal gels can be compared to the copper alginate gel obtained by (Agulhon et al., 2014) where both alginate and divalent cations concentrations were fixed to $20\,g\,L^{-1}$ and 100 mM, respectively. They have found that the gels prepared with Cu^{2+} (100 mM) had the higher G' value (51 kPa), whereas, for Co^{2+} and Mn^{2+}, the G' was smaller (5 and 2 kPa) and was frequency dependent.

3.3. Measurement of the gel front migration

Fig. 4 presents the spatiotemporal variation of the transmittance intensity during the diffusion of divalent cations (Mg^{2+}, Zn^{2+}, Ca^{2+} and Ba^{2+}) through a dialysis membrane into a polyGal solution (set up presented in Fig. 1). Before adding divalent cations (t = 0 min), the transmittance intensity of polyGal solution was around 80% which indicated that the solution was slightly turbid and stable all along the tube. As the gelation time increased, the divalent cations (X^{2+}) diffused through the dialysis membrane and interacted with galacturonate units. These interactions induced changes in the turbidity of the mixture (Fig. 4). When the transmittance intensity was around 80 %, the cation-polyGal mixture was considered in a liquid state (part from 0 to 30 mm in Fig. 4). The decrease of this value at a low distance may be associated

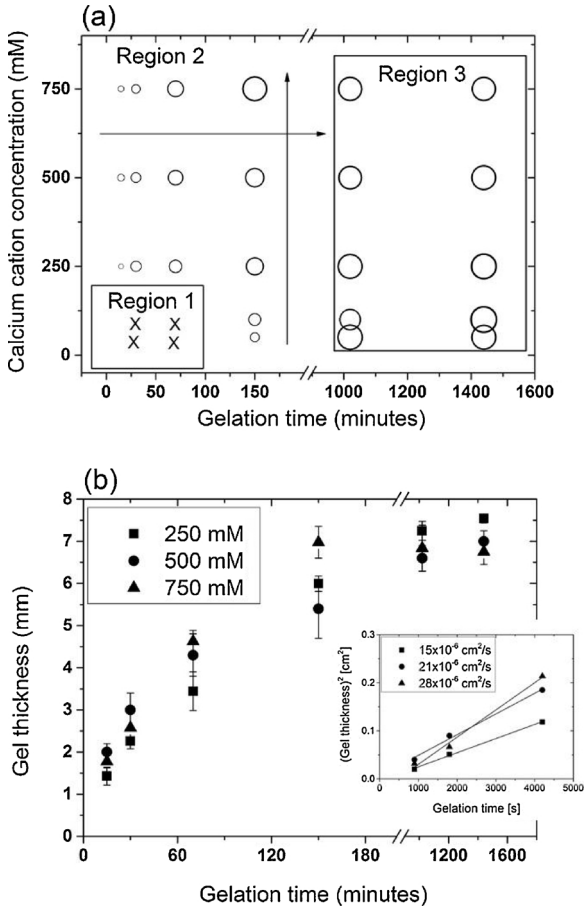

Fig. 2. (a) evolution of the gel thickness as a function of the gelation time for Ca-polyGal gel. The concentration of polyGal was fixed at 10 g L^{-1} (54 mM galacturonic unit). The cross symbols represent samples where the thickness was too low to be measured (the gel was brittle). The diameter of circles is related to the gel thickness (as the gel thickness increased, the diameter of the circle increased as shown by the arrows). (b) evolution of the gel thickness (d) of the Ca-polyGal gel as a function of the gelation time for three initial calcium concentrations. The insert in (b) corresponds to the linear fit of the square of gel thickness [cm^2] versus the gelation time [s]. The evolution of gel thickness for the two others divalent cations (Ba^{2+} and Zn^{2+}) is presented in Fig. S1 in the Supplementary information.

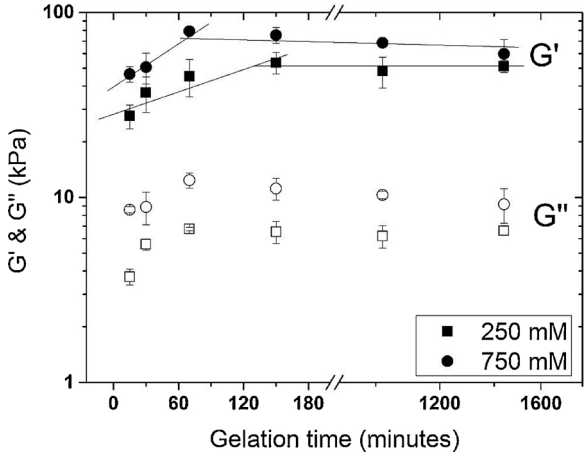

Fig. 3. Evolution of the elastic modulus, G', (full symbols) and viscous modulus, G", (empty symbols) of Ca-polyGal gels at two initial Ca^{2+} concentration (250 mM and 750 mM). The measurements were performed in triplicate at fixed temperature, stress and frequency (25 °C, τ = 50 Pa and ω = 10 rad s^{-1}, respectively). Lines are to guide eyes.

with the formation of a gel in the case of Zn^{2+}, Ca^{2+} and Ba^{2+}. Thus, the sol-gel transition (gel front) can be correlated to the beginning of the decrease of the transmittance intensity. Before this decrease, we have observed a peak with a high transmittance intensity (around 100%) which was due to a change in the refractive index between two phases and could be attributed to a local depletion of polymer chains as interpreted by Braschler et al. (2011). Indeed, they have shown that the depletion zone can be located by a dip in the fluorescence intensity profile. As the gelation time increased, the peak observed in the turbidity profile was shifted to large distances (Fig. 4a–c). The distance from the dialysis membrane to this peak could correspond to the thickness of the gel layer (*d*) and thus to the gel front migration distance. In the gel zone *(d)*, some fluctuations in the turbidity were observed (Fig. 4a–c). These fluctuations remained at the same position and could be due to the presence of some macroscopic heterogeneities in the gel. In iron(II)-polyGal gels, gradients of both polymer concentration and Young modulus were observed following the direction of the reaction zone (Maire du Poset et al., 2018). However, the local organization of the polyGal chain's network remained identical all along the hydrogel (the mesh size of the gel is about 7.5 nm). Thus the progressive decrease of chains concentration was attributed to the existence of heterogeneities at mesoscopic scale with the presence of low density zones within the gel (Maire du Poset et al., 2018). When magnesium ions are in contact with the polyGal solution, a jump of the transmittance is observed indicating that the Mg-polyGal mixture became turbid (Fig. 4d). The increase of the turbidity could be due to the formation of some aggregates caused by an increase of the ionic strength. Indeed, the interaction of Mg^{2+} with polyGal is a weak process (non-gelling) governed by only electrostatic interactions (Selvarengan, Kubicki, Guégan, & Châtellier, 2010) and it can be attributed to the polycondensation process (. Donati, Cesaro, & Paoletti, 2006; Manning, 1977). Thus, the transmittance jump could be attributed to the transition between the polyGal solution and the aggregated domains. The observed transmittance jump was shifted to large distance and could be associated to the magnesium cations diffusion (Fig. 4d).

Skjåk-Bræk et al. (1989) have suggested a gelation model based on the theory developed by Sherwood & Pigford, 1952 allowing to calculate the diffusion coefficient (D) of calcium ions through the gel network provided that the diffusion of the polysaccharide molecules is very low. Furthermore, they have assumed that the polysaccharide gelation by calcium ions is stoichiometric, irreversible and very rapid compared to the rate of diffusion of the reactants (Sherwood & Pigford, 1952; Skjåk-Bræk et al., 1989). Thus, the dependence of the d^2 (squared gel thickness) was proportional to the gelation time (*t*), implying that the gelation process was diffusion limited (Potter et al., 1994). In the present study, a linear relationship between the square gel thickness (d^2) and the gelation time (*t*) was observed (Fig. 5a). According to the theory of free molecular diffusion, the dependence of *d* on *t* is given by the equation $d^2 = 2D_{app}t$ (Sherwood & Pigford, 1952). The apparent diffusion for the four divalent cations (Mg^{2+}, Zn^{2+}, Ca^{2+} and Ba^{2+}) are listed in Table 1. For Mg-polyGal, the calculated diffusion coefficient can be attributed to the transition between the polyGal solution and aggregated domains and not to the gel front migration. It can be observed that the diffusion coefficients of the gel front (D_{app}) increased with the initial concentration of the divalent cations (Fig. 5b). The same trend was observed in previous studies with other anionic polysaccharides (Bjørnøy et al., 2016; Kim, 1990; Potter et al., 1994; Wu et al., 2014). Kim showed that the diffusion coefficient increased with increasing calcium ions concentration, and he attributed this to the formation of macropores (~10 μm) at high calcium concentration (> 125 mM) (Kim, 1990). More recently, Caccavo et al. have presented a quantitative approach to describe the formation of capillarity during the gelation process of calcium-alginate systems (Caccavo et al., 2016) and have shown that the higher the ionic concentration, the longer were the capillaries (Potter et al., 1994). Based on the mass balance of ions in the gelling zone, Skjåk-Bræk et al. (1989) have proposed the

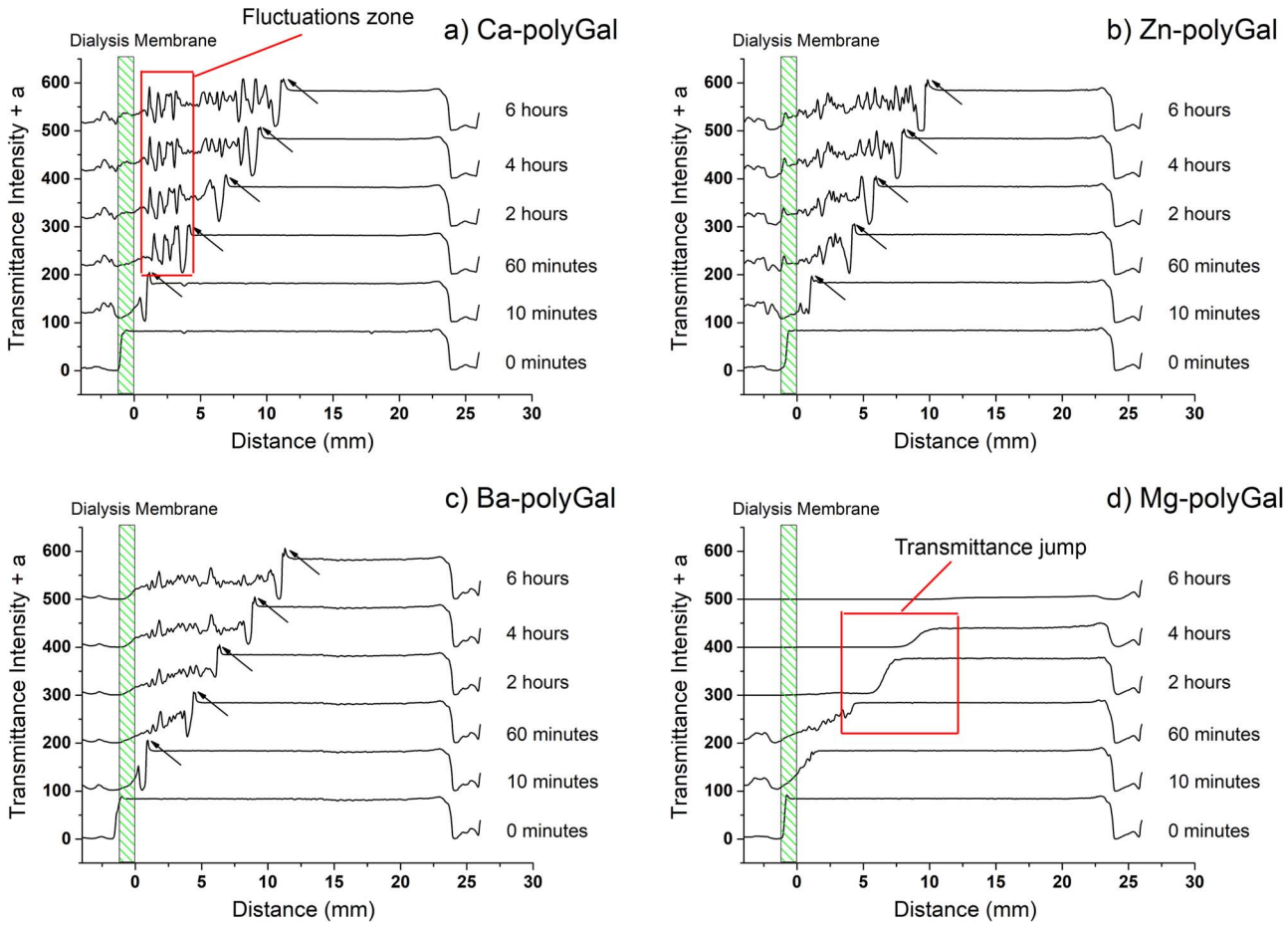

Fig. 4. Evolution of the transmittance intensity in the polyGal solution as a function of the height of the tube (distance) and the gelation time for Ca^{2+}, Zn^{2+}, Ba^{2+} and Mg^{2+}. The diffusion of divalent cations occurred from the left side to the right one from the dialysis membrane. The arrows represent the transition sol-gel (gel front).

following equation $D_{app} = (C_s/C_g)\ D$; where C_s, C_g and D are the concentration of cations in the solution, the concentration of cations required for the gelation and the diffusion coefficient of the divalent cations in the gel, respectively. It can be noted that the diffusion of ions in porous gels is reduced compared to that in water (Skjåk-Bræk et al., 1989; Ström et al., 2007). Nobe, Dobashi, and Yamamoto (2005) have found that the diffusion coefficient of calcium inside curdlan gel was 4 times lower than the diffusion coefficient of calcium cation in pure water; they have attributed this to the effect of an excess amount of friction resulting from curdlan network of the gel. The diffusion coefficients of the four divalent cations in pure water (D_0) at 25 °C are 7.4×10^{-6}; 8.5×10^{-6}; 7.0×10^{-6}; and $7.1 \times 10^{-6}\ cm^2\ s^{-1}$ for Ca^{2+}, Zn^{2+}, Ba^{2+} and Mg^{2+}, respectively (Hazel & Sidell, 1987; Weast, Astle, & Beyer, 1986). As shown in Table 1, the increase of divalent cation concentration induced an increase of D_{app} which was in accordance with previous studies (Bjørnøy et al., 2016; Braschler et al., 2011; Kim, 1990; Potter et al., 1994; Wu et al., 2014). When the concentration of divalent cation (C_s) increased from 50 to 250 mM, the D_{app} increased ~5 times (Table 1). The concentration of cation required for the gelation (C_g) can be estimated from the initial concentration of the

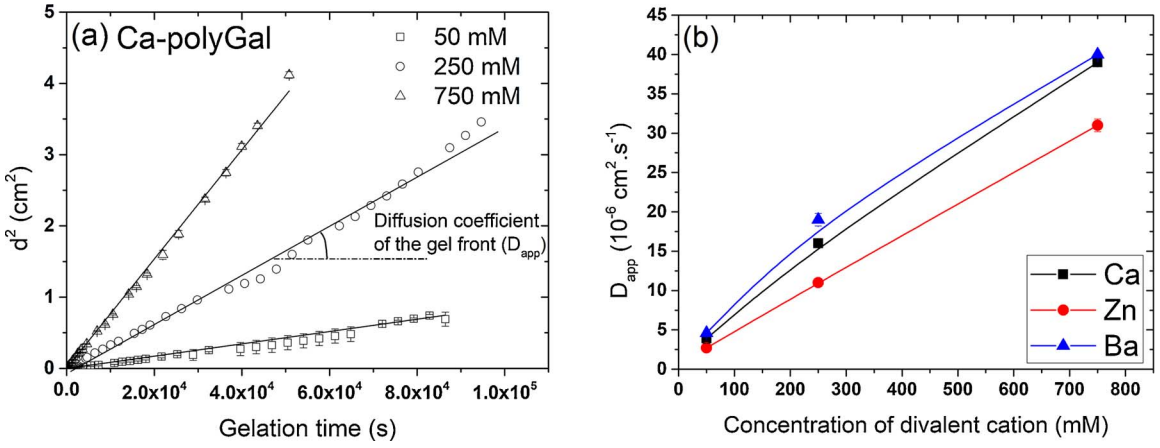

Fig. 5. (a) Evolution of the square of the gel thickness, d^2, versus gelation time, t, of Ca-polyGal gels at three various calcium concentrations. (b) Evolution of the gel front diffusion coefficient as a function of the initial cation concentration for the three divalent cations (Zn^{2+}, Ca^{2+} and Ba^{2+}).

Table 1
Diffusion coefficients of the gel front (D_{app}) and of the cation in the gel (D) for each divalent cation (Zn^{2+}, Ca^{2+}, and Ba^{2+}) at three cation concentrations (50, 250 and 750 mM). D_0 is the diffusion coefficient of the divalent cation in pure water.

Type of gel	$[X^{2+}]_s$,mM	Diffusion coefficient of the gel front (D_{app}), $10^{-6}\,cm^2\,s^{-1}$	Diffusion coefficient of divalent cation in the gel (D), $10^{-6}\,cm^2\,s^{-1}$	D/D_0
Ca-polyGal	50	3.9 ± 0.6	1.1	7
	250	16.0 ± 0.4	0.9	8
	750	39.0 ± 0.5	0.7	10
Zn-polyGal	50	2.7 ± 0.2	0.7	11
	250	11.0 ± 0.5	0.6	14
	750	31.0 ± 0.8	0.6	15
Ba-polyGal	50	4.6 ± 0.1	1.3	6
	250	19.0 ± 0.8	1.0	7
	750	40.0 ± 0.1	0.7	10

polyGal ($10\,g\,L^{-1}$). In a recent study, it was shown that the molar ratio in polyGal gels induced by iron(II) remained constant along the gel ($R = [X^{2+}]/[Gal\ units] = 0.25$) (Maire du Poset et al., 2018). This was also demonstrated for two divalent cations (Ca^{2+} and Zn^{2+}) (data not published yet). Thus, C_g was then equal to 13.75 mM (Gal unit concentration was 55 mM). By assuming that the C_s remained constant during the gelation process, we can determine the coefficient diffusion of the cation in the gel (D) (Table 1). For the three divalent cations (Zn^{2+}, Ca^{2+} and Ba^{2+}), D was about ten times lower than the diffusion coefficient of the cation in pure water ($0.7–1.3 \times 10^{-6}\,cm^2\,s^{-1}$). Moreover, D decreased as the divalent cation concentration increased (for Ca^{2+} and Ba^{2+}); while for Zn-polyGal, D remained constant. We have recently shown that the mechanism of binding divalent cations (Zn^{2+}, Ca^{2+} and Ba^{2+}) to polyGal, in the dilute regime, depends on the affinity of the cation for its water molecules shell. This affinity increased following the given order: $Ba^{2+} < Ca^{2+} < Zn^{2+}$ (Huynh, Lerbret, Neiers, Chambin, & Assifaoui, 2016). The greater this affinity is, the more difficult the interaction between cations and polyGal is. This may explain the low diffusion coefficient of Zn^{2+} in the gel.

4. Discussion

The polyGal gel growth process was evaluated by the determination of the spatiotemporal variation of the turbidity by using a Turbiscan® apparatus. In the case of Zn-polyGal, Ca-polyGal and Ba-polyGal, a consistent gel was formed. The evolution of the transmittance showed the presence of a peak at the gel front. This peak which corresponds to the sol/gel transition is due to changes in the refractive index between the polyGal solution and the polyGal gel. According to Braschler et al. (2011), we have attributed this peak to a local depletion of polymer chains. In the case of the diffusion of divalent cation without any gel formation (Mg-polyGal), we didn't observe any peak at the interface (Fig. 4b) indicating that the presence of the peak is not an artefact and it is really associated to the gel front. For Mg-polyGal, we have noticed a transmittance jump due to the transition between the polyGal solution and the aggregated domains. In our recent study (Huynh et al., 2016), we have suggested that the Mg^{2+} cation interacted so strongly with its hydration shell hindering the formation of monocomplexes which is the first step in the gelation mechanism as proposed by Fang et al. (Fang et al., 2007). Thus, the polycondensation phenomenon may be due to the water molecules sharing from the first coordination shell of Mg^{2+} and the carboxylate groups of polyGal (Huynh et al., 2016).

The position of the peak at the gel front allowed us to determine the apparent diffusion coefficient (D_{app}) of the gel front. Moreover, the diffusion coefficient values obtained by the gel thickness determination method (method 1) and by using the Turbiscan apparatus (method 2) were quite similar and increased with the initial calcium concentration. When the calcium concentration was changed from 250 to 750 mM, the obtained D_{app} was almost doubled with both methods (for method 1, D_{app} increased from 15 to $29 \times 10^{-6}\,cm^2\,s^{-1}$ and for method 2, D_{app} increased from 17 to $39 \times 10^{-6}\,cm^2\,s^{-1}$). It can be noted that the obtained D_{app} values were in the same range as those obtained for calcium-curdlan (Dobashi, Nobe, Yoshihara, Yamamoto, & Konno, 2004) or for calcium-poly(2,20-disulfonyl-4,40-benzidine terephthalamide) systems (Wu et al., 2011).

For low gelation time ($t \le t_p$), the gel density (Eq. (1)) was low and stable (data are not shown); while the thickness, G' and G" of the gel continued to increase (Figs. 2b and 4). The increase of the elastic modulus may be due to the increase in the number of crosslinked polymers chains. At a fixed divalent cation concentration (250 mM), the t_p seemed to be constant (~ 150 min) whatever the nature of divalent cation (Fig. 3); while, the diffusion coefficient was cation-dependent and was equal to 11, 16 and $19\,cm^2\,s^{-1}$ for Zn^{2+}, Ca^{2+} and Ba^{2+}, respectively (Table 1). As the gelation time increased ($t > t_p$), both the gel density and the viscoelastic properties became higher and did not evolve significantly indicating that the gelation was achieved. The establishment of the cation-polysaccharide network depended on the molar ratio, ($R = [X^{2+}]/[GalA]$) (Fang et al., 2007; Ventura et al., 2013). Moreover, we have recently shown, in the diluted regime, the presence of a threshold molar ratio (R*) which was linked to the number and the flexibility of the crosslinks (Huynh et al., 2016). When the crosslinks were low or high flexibles, the formation of dimers was shifted to the high molar ratio (R*). For the three types of hydrogels

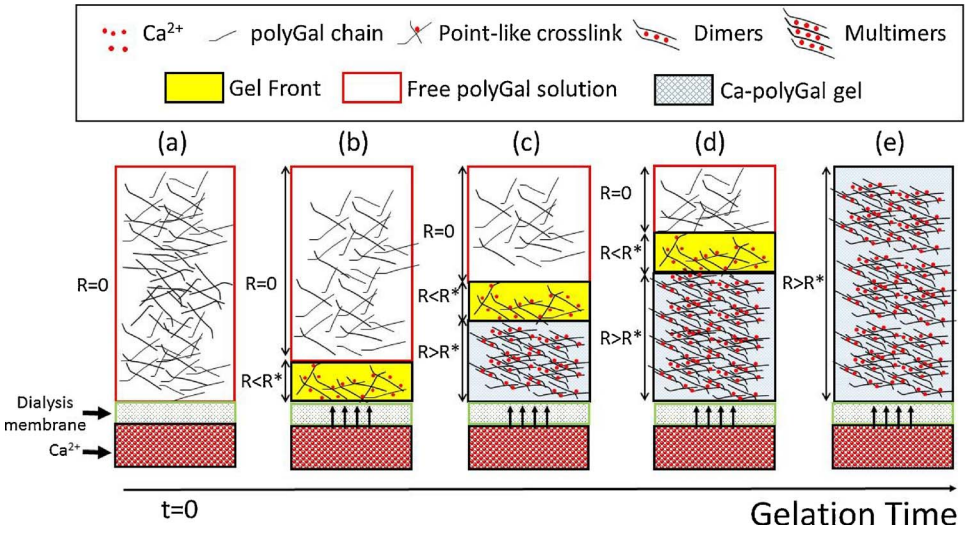

Fig. 6. Schema for the gelation process of polyGal solution (a). First, calcium cations diffused through the dialysis membrane and interacted with carboxylate groups of the polyGal. This allowed the formation of many point-like crosslinks which were located near the dialysis membrane (b). When the molar ratio was higher than R*, these point-like crosslinks became dimers and multimers (c–e). This induced a contraction of the polymer chains and thus the formation of the gel front. The gelation was achieved in (e).

(Zn-polyGal, Ca-polyGal and Ba-polyGal), the gel density became higher with the gelation time which is correlated to the molar ratio (R).

During the gelation process, we suggested the presence of two successive steps which are time-dependent (Fig. 6): i) the diffusion of divalent cations induced the formation of monocomplexes and some point-like crosslinks (Gal-Ca-Gal) (Borgogna, Skjåk-Bræk, Paoletti, & Donati, 2013; Huynh et al., 2016; Ventura et al., 2013). ii) for the higher molar ratio (R > R*), the increase of calcium ions concentration induced the formation of dimers (junction zones) and multimers (lateral association of dimers) (Huynh et al., 2016). The formation of these dimers and multimers could improve the gel density and induced an internal stress that created a depletion zone at the sol-gel interface (Wu et al., 2014). The gel front migration was fast when the initial calcium cation concentration was high (Fig. 5). Thus, we can conclude that for high calcium concentrations, the two steps (i) and (ii) were very close in time. The step (i) could be considered as a precursor for the formation of dimers and multimers in the second step (ii). For the two others divalent cations (Ba^{2+} and Zn^{2+}), the gelation process could be described by these two steps but with different gelation kinetics. Recent molecular dynamics simulations studies have shown that Ba^{2+} contribute to the creation of a high number of crosslinks (Gal-Ba-Gal) with low stability; while Zn^{2+} contribute to the creation a low number of crosslinks (Gal-Zn-Gal) with high stability (Huynh et al., 2016). We assumed that high stable crosslinks slow down the formation of dimers and multimers. This can explain the high-speed gel front migration observed for Ba-polyGal in comparison with Zn-polyGal (Fig. 5b).

5. Conclusion

The diffusion of calcium ions into a polyGal solution through a dialysis membrane allowed the formation of a Ca-polyGal gel. As the gelation time increased, both the thickness of the gel and the viscoelastic properties (G' and G") increased. Moreover, changes in the turbidity of the polyGal solution during the gelation process were observed. Thus, by using a Turbiscan apparatus, the evolution of the gel front was visualized and studied as a function of the gelation time. We have demonstrated that the gel front can be characterized by a peak in the turbidity profile. This peak corresponded to a change in the refractive index between the polyGal solution and the Ca-polyGal gel. The study of three other divalent cations (Mg^{2+}, Zn^{2+}, Ba^{2+}) confirmed these conclusions. Indeed, we have observed a peak at the gel front for Zn-polyGal and Ba-polyGal gels. While for Mg-polyGal mixture, the gel was not formed and in this case, only a transmittance jump was observed due to a transition between the polyGal solution and aggregated domains. For a given gelation time, the diffusion of X^{2+} induced an increase of the molar ratio. We suggested that for the low molar ratio (R = [Cation]/[Galacturonate unit]), monocomplexes and point-like crosslinks were formed. When the number and the flexibility of these crosslinks are adequate (R = R*), the formation of dimers and multimers will occur. In addition, we have calculated the gel front diffusion coefficients (D_{app}) and have found that D_{app} increased when the initial calcium concentration was increased which was in line with previous studies. The diffusion coefficient of gel front for Zn-polyGal was lower than that of Ca-polyGal and Ba-polyGal. This could be attributed to the high stability of crosslinks formed in the case of Zn^{2+} in comparison with the two other cations (Ca^{2+} and Ba^{2+}).

Conflict of interests

The authors declare no competing financial interest.

Acknowledgements

This work is supported by the Conseil Régional de Bourgogne through the plan d'actions régional pour l'innovation (PARI ALIM+) and the European Union through the PO FEDER-FSE Bourgogne 2014/2020 programs. The viscoelastic properties and turbidity measurements were determined with equipment from the technical platform RMB (Rhéologie et structure des Matériaux Biologiques) (AgroSup Dijon, Université de Bourgogne Franche-Comté). We are grateful to Dr Adrien LERBRET (UMR, PAM, AgroSup Dijon) for critical reading and comments on the manuscript.

Appendix A. Supplementary data

Supplementary data associated with this article can be found, in the online version, at https://doi.org/10.1016/j.carbpol.2018.02.046.

References

Agulhon, P., Robitzer, M., Habas, J.-P., & Quignard, F. (2014). Influence of both cation and alginate nature on the rheological behavior of transition metal alginate gels. *Carbohydrate Polymers, 112*, 525–531.

Assifaoui, A., Chambin, O., & Cayot, P. (2011). Drug release from calcium and zinc pectinate beads: impact of dissolution medium composition. *Carbohydrate Polymers, 85*, 388–393.

Assifaoui, A., Lerbret, A., Uyen, H. T. D., Neiers, F., Chambin, O., Loupiac, C., et al. (2015). Structural behaviour differences in low methoxy pectin solutions in the presence of divalent cations (Ca^{2+} and Zn^{2+}): A process driven by the binding mechanism of the cation with the galacturonate unit. *Soft Matter, 11*, 551–560.

Bjørnøy, S. H., Mandaric, S., Bassett, D. C., Åslund, A. K. O., Ucar, S., Andreassen, J.-P., et al. (2016). Gelling kinetics and in situ mineralization of alginate hydrogels: A correlative spatiotemporal characterization toolbox. *Acta Biomaterialia, 44*, 243–253.

Borgogna, M., Skjåk-Bræk, G., Paoletti, S., & Donati, I. (2013). On the initial binding of alginate by calcium ions. The tilted Egg-Box hypothesis. *The Journal of Physical Chemistry B, 117*, 7277–7282.

Braschler, T., Valero, A., Colella, L., Pataky, K., Brugger, J., & Renaud, P. (2011). Link between alginate reaction front propagation and general reaction diffusion theory. *Analytical Chemistry, 83*, 2234–2242.

Bru, P., Brunel, L., Buron, H., Cayré, I., Ducarre, X., Fraux, A., et al. (2004). *Particle size and rapid stability analyses of concentrated dispersions: Use of multiple light scattering technique. Particle sizing and characterization*. American Chemical Society45–60.

Caccavo, D., Ström, A., Larsson, A., & Lamberti, G. (2016). Modeling capillary formation in calcium and copper alginate gels. *Materials Science and Engineering: C, 58*, 442–449.

Dobashi, T., Nobe, M., Yoshihara, H., Yamamoto, T., & Konno, A. (2004). Liquid crystalline gel with refractive index gradient of curdlan. *Langmuir, 20*, 6530–6534.

Donati, I., Cesaro, A., & Paoletti, S. (2006). Specific interactions versus counterion condensation: 1. Nongelling ions/polyuronate systems. *Biomacromolecules, 7*, 281–287.

Donati, I., Asaro, F., & Paoletti, S. (2009). Experimental evidence of counterion affinity in alginates: The case of nongelling ion Mg^{2+}. *Journal of Physical Chemistry B, 113*, 12877–12886.

Fang, Y., Al-Assaf, S., Phillips, G. O., Nishinari, K., Funami, T., Williams, P. A., et al. (2007). Multiple steps and critical behaviors of the binding of calcium to alginate. *The Journal of Physical Chemistry B, 111*, 2456–2462.

Hazel, J. R., & Sidell, B. D. (1987). A method for the determination of diffusion coefficients for small molecules in aqueous solution. *Analytical Biochemistry, 166*, 335–341.

Hills, B. P., Godward, J., Debatty, M., Barras, L., Saturio, C. P., & Ouwerx, C. (2000). NMR studies of calcium induced alginate gelation. Part II. The internal bead structure. *Magnetic Resonance in Chemistry, 38*, 719–728.

Huynh, U. T. D., Lerbret, A., Neiers, F., Chambin, O., & Assifaoui, A. (2016). Binding of divalent cations to polygalacturonate: A mechanism driven by the hydration water. *The Journal of Physical Chemistry B, 120*, 1021–1032.

Kim, H.-S. (1990). A kinetic study on calcium alginate bead formation. *Korean Journal of Chemical Engineering, 7*, 1–6.

Li, J., & Mooney, D. J. (2016). Designing hydrogels for controlled drug delivery. *Nature Reviews, 1*, 16071.

Mørch, Ý. A., Donati, I., & Strand, B. L. (2006). Effect of Ca^{2+}, Ba^{2+}, and Sr^{2+} on alginate microbeads. *Biomacromolecules, 7*, 1471–1480.

Maire du Poset, A., Lerbret, A., Zitolo, A., Cousin, F., & Assifaoui, A. (2018). Design of polygalacturonate hydrogels using iron(II) as crosslinkers: A promising route to protect bioavailable iron against oxidation. *Carbohydrate Polymers, 188*, 276–283. http://dx.doi.org/10.1016/j.carbpol.2018.1002.1007.

Maki, Y., Ito, K., Hosoya, N., Yoneyama, C., Furusawa, K., Yamamoto, T., et al. (2011). Anisotropic structure of calcium-induced alginate gels by optical and small-angle X-ray scattering measurements. *Biomacromolecules, 12*, 2145–2152.

Maki, Y., Furusawa, K., Yasuraoka, S., Okamura, H., Hosoya, N., Sunaga, M., et al. (2014). Universality and specificity in molecular orientation in anisotropic gels prepared by diffusion method. *Carbohydrate Polymers, 108*, 118–126.

Maki, Y., Furusawa, K., Dobashi, T., Sugimoto, Y., & Wakabayashi, K. (2017). Small-angle X-ray and light scattering analysis of multi-layered curdlan gels prepared by a diffusion method. *Carbohydrate Polymers, 155*, 136–145.

Manning, G. S. (1977). Limiting laws and counterion condensation in polyelectrolyte solutions: IV. The approach to the limit and the extraordinary stability of the charge fraction. *Biophysical Chemistry, 7*, 95–102.

Nobe, M., Dobashi, T., & Yamamoto, T. (2005). Dynamics in dialysis process for liquid crystalline gel formation. *Langmuir, 21*, 8155–8160.

Potter, K., Balcom, B. J., Carpenter, T. A., & Hall, L. D. (1994). The gelation of sodium

alginate with calcium ions studied by magnetic resonance imaging (MRI). *Carbohydrate Research, 257*, 117–126.
Selvarengan, P., Kubicki, J. D., Guégan, J. P., & Châtellier, X. (2010). Complexation of carboxyl groups in bacterial lipopolysaccharides: Interactions of H^+, Mg^{2+}, Ca^{2+}, Cd^{2+}, and UO_2^{2+} with Kdo and galacturonate molecules via quantum mechanical calculations and NMR spectroscopy. *Chemical Geology, 273*, 55–75.
Sherwood, T. K., & Pigford, R. L. (1952). *Absorption and extraction.* New York-London: McGraw-Hill.
Skjåk-Bræk, G., Grasdalen, H., & Smidsrød, O. (1989). Inhomogeneous polysaccharide ionic gels. *Carbohydrate Polymers, 10*, 31–54.
Stokke, B. T., Draget, K. I., Smidsrød, O., Yuguchi, Y., Urakawa, H., & Kajiwara, K. (2000). Small angle X-ray scattering and rheological characterization of alginate gels. 1. Ca-alginate gels. *Macromolecules, 33*, 1853–1863.
Ström, A., Ribelles, P., Lundin, L., Norton, I., Morris, E. R., & Williams, M. A. K. (2007). Influence of pectin fine structure on the mechanical properties of calcium-pectin and acid-pectin gels. *Biomacromolecules, 8*, 2668–2674.
Thibault, J. F., & Rinaudo, M. (1985). Interactions of mono- and divalent counterions with alkali- and enzyme-deesterified pectins in salt-free solutions. *Biopolymers, 24*, 2131–2143.
Thu, B., Gåserød, O., Paus, D., Mikkelsen, A., Skjåk-Bræk, G., Toffanin, R., et al. (2000). Inhomogeneous alginate gel spheres: An assessment of the polymer gradients by synchrotron radiation-induced x-ray emission, magnetic resonance microimaging and mathematical modeling. *Biopolymers, 53*, 60–71.
Vashist, A., Vashist, A., Gupta, Y. K., & Ahmad, S. (2014). Recent advances in hydrogel based drug delivery systems for the human body. *Journal of Materials Chemistry B, 2*, 147–166.
Ventura, I., Jammal, J., & Bianco-Peled, H. (2013). Insights into the nanostructure of low-methoxyl pectin–calcium gels. *Carbohydrate Polymers, 97*, 650–658.
Weast, R. C., Astle, M. J., & Beyer, W. H. (1986). *CRC handbook of chemistry and physics* (66th ed.). Florida, USA: CRC Press.
Wu, Z. L., Kurokawa, T., Sawada, D., Hu, J., Furukawa, H., & Gong, J. P. (2011). Anisotropic hydrogel from complexation-driven reorientation of semirigid polyanion at Ca^{2+} diffusion flux front. *Macromolecules, 44*, 3535–3541.
Wu, Z. L., Takahashi, R., Sawada, D., Arifuzzaman, M., Nakajima, T., Kurokawa, T., et al. (2014). In situ observation of Ca^{2+} diffusion-induced superstructure formation of a rigid polyanion. *Macromolecules, 47*, 7208–7214.